

# Controllable Neural Architectures for Multi-Task Control

Umberto Casti, Giacomo Baggio, Sandro Zampieri, and Fabio Pasqualetti

**Abstract**—This paper studies a multi-task control problem where multiple linear systems are to be regulated by a single non-linear controller. In particular, motivated by recent advances in multi-task learning and the design of brain-inspired architectures, we consider a neural controller with (smooth) ReLU activation function. The parameters of the controller are a connectivity matrix and a bias vector: although both parameters can be designed, the connectivity matrix is constant while the bias vector can be varied and is used to adapt the controller across different control tasks. The bias vector determines the equilibrium of the neural controller and, consequently, of its linearized dynamics. Our multi-task control strategy consists of designing the connectivity matrix and a set of bias vectors in a way that the linearized dynamics of the neural controller for the different bias vectors provide a good approximation of a set of desired controllers. We show that, by properly choosing the bias vector, the linearized dynamics of the neural controller can replicate the dynamics of any single, linear controller. Further, we design gradient-based algorithms to train the parameters of the neural controller, and we provide upper and lower bounds for the performance of our neural controller. Finally, we validate our results using different numerical examples.

## I. INTRODUCTION

Control algorithms are typically tuned to optimize the performance of a single dynamical system. Similarly, machine learning algorithms are often trained for specific datasets and require time-consuming retraining procedures to accommodate changes in the data and objectives [1], [2]. On the other hand, many natural systems can seamlessly adapt across different tasks and transfer learned skills to new and unseen contexts. In the human brain, for instance, astrocytes are believed to bias neuronal functioning to provide contextual adaptation capabilities [3] without changing neuronal coupling. Motivated by the discrepancy between natural and artificial systems and the need to alleviate retraining times and requirements, techniques for multi-task learning have recently been developed [4], [5], showing that a single artificial architecture can in fact learn to solve multiple tasks. Yet, techniques for multi-task control have remained elusive.

In this paper, we propose a non-linear neural controller to solve a multi-task control problem. We consider a controller inspired by neural architectures [6] with (smooth) ReLU activation function (see Fig. 1). The parameters of the controller are the states connectivity matrix, whose value is trained at design time and remains constant, and a bias vector, whose

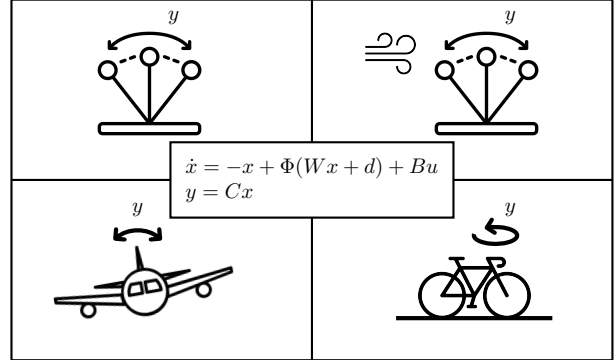


Fig. 1. An illustration of the multi-task control problem considered in this paper, where a set of linear systems is to be regulated by a single non-linear controller. This paper proposes a neural controller with (smooth) ReLU activation function and two parameters. The connectivity matrix  $W$  is typically large and remains constant across the different tasks. The bias vector  $d$ , instead, is low-dimensional and is used to adapt the performance of the neural controller to different control tasks. See Section II for a detailed explanation of the neural controller and our multi-task control problem, and Section III for a numerical study of this multi-task control example.

value depends on the control problem at hand and is selected among a set of values trained at design time. Selecting the bias vector is a convenient way to provide the controller with the ability to adapt to different dynamical systems and tasks without the need to retrain the states connectivity matrix. We emphasize that the main objective of this work is to validate the ability of our nonlinear controller to approximate the behavior of a set of desired linear controllers, rather than to solve any specific control problem. Loosely speaking, our approach takes inspiration from the human brain that, despite a relatively static neuronal network, modulates neuronal responses to accommodate contextual and task changes.

**Related Work.** The literature on multi-task control is limited. Traditional controller design methods, such as the linear quadratic regulator and model predictive control [7], [8], are tailored for single dynamical systems and often require a complete redesign when system dynamics change.

Adaptive control is crucial for managing systems with significant uncertainties, where robust techniques fail [9]. These frameworks typically employ a family of controllers with parameters that vary smoothly [10]. However, when system parameters affect dynamics in complex ways, constructing a continuously parameterized set of controllers becomes difficult, especially if high robustness and performance are required. To mitigate these challenges, approaches like logic-based switching strategies [11]–[13] have been proposed, focusing on discrete controller switching rather than continuous adjustments. Our work, in contrast, studies the approximation

This material is based upon work supported in part by awards AFOSR-FA9550-20-1-0140, and AFOSR-FA9550-19-1-0235. Fabio Pasqualetti are with the Department of Mechanical Engineering, University of California at Riverside, [fabiopas@ucr.edu](mailto:fabiopas@ucr.edu). Umberto Casti, Giacomo Baggio, and Sandro Zampieri are with the Department of Information Engineering, University of Padova, Italy [castiumber,baggio,zampi}@dei.unipd.it](mailto:{castiumber,baggio,zampi}@dei.unipd.it)

properties of a neural controller, which is independent but could be integrated with such switching-based methods.

Recent studies in multi-task control, such as [14], [15], explore system identification across multiple datasets, while others [16], [17] address transfer and imitation control. Differently from these approaches, this paper considers a setting where the system to be controlled varies abruptly and arbitrarily.

Multi-task learning methods enable neural networks to handle diverse problems, often employing techniques like masks to select task-specific network components [4]. However, these methods are prone to catastrophic forgetting, where models lose previously learned knowledge when exposed to new tasks [18], [19]. Despite the extensive literature on multi-task learning [4], [5], [20], [21], such techniques do not directly address control challenges or provide performance guarantees.

The work most similar to ours is [22], which studies simultaneous approximation of multiple systems using a single approximating model. In contrast, our method allows for multiple approximating systems that share a common connectivity matrix but differ through low-dimensional bias vectors. This relationship between systems introduces complexity, making existing LMI techniques [22] inapplicable in a straightforward manner.

Finally, our architecture draws inspiration from neuroscience, particularly the interplay between astrocytes and neurons in the human brain [23]–[25]. Emerging theories suggest that astrocytes modulate neuronal function, enabling adaptive responses without altering the network structure [3]. Our neural controller mimics this biological mechanism, where the bias vector acts analogously to astrocytic modulation, facilitating context-dependent adaptation.

**Paper contribution.** The main contributions of this paper are as follows. First, we formulate a novel multi-task control problem, where a set of known linear systems is to be regulated by a (possibly varying) single controller. We propose a novel control strategy based on a non-linear neural controller with (smooth) ReLU activation function and two parameters: a connectivity matrix and a bias vector. While the controller connectivity matrix is trained at design stage and remains constant, the values of the low-dimensional bias vector are trained at design stage but can vary over time. Changing the bias vector modifies the equilibria of the neural controller and its linearized dynamics, and allows the controller to approximate different desired linear dynamics by tuning a small subset of the parameters. Second, we prove that, by properly choosing the bias vector, the linearized dynamics of the neural controller can replicate the dynamics of any linear system. Third, we provide a gradient-based algorithm to train the parameters of the neural controllers in a way that its linearized dynamics obtained by appropriately changing the bias vector approximate a set of desired linear dynamics. Fourth and finally, we provide upper and lower bounds on the performance of our multi-task control problem. While some bounds are of technical nature, others show of the approximation capabilities of the neural controller depend on

the dimension, number and similarity of the desired linear dynamics, and the dimension of the neural controller.

**Paper organization.** The rest of the paper is organized as follows. Section II contains our problem formulation and preliminary results. Section III contains our numerical algorithms and some numerical results. Finally, Section IV contains our lower and upper bounds on the multi-task control problem, and Section V concludes the paper.

## II. PROBLEM SETUP AND PRELIMINARY NOTIONS

Consider the following non-linear neural controller:

$$\Sigma = \begin{cases} \dot{x} = -x + \Phi(Wx + d) + Bu, \\ y = Cx, \end{cases} \quad (1)$$

where  $x \in \mathbb{R}^N$ ,  $d \in \mathbb{R}^N$ ,  $u \in \mathbb{R}^m$ , and  $y \in \mathbb{R}^p$  are the state, a free parameter, input, and output of the controller, respectively, and  $W \in \mathbb{R}^{N \times N}$ ,  $B \in \mathbb{R}^{N \times m}$  and  $C \in \mathbb{R}^{p \times N}$  are the controller matrices. The activation function  $\Phi: \mathbb{R}^N \rightarrow (0, +\infty)^N$  is the elementwise application of the (smooth) ReLU function  $\phi: \mathbb{R} \rightarrow (0, +\infty)$ , which is defined as  $\phi(x) = \ln(1 + e^x)$ . Further, when  $u = 0$ , the equilibria of the neural controller (1) satisfy the equation

$$x_{\text{eq}} = \Phi(Wx_{\text{eq}} + d), \quad (2)$$

and, locally, obey the linearized dynamics

$$\Sigma^L = \left( -I + \underbrace{\text{diag}(\Phi_d(Wx_{\text{eq}} + d))}_D W, B, C \right), \quad (3)$$

where  $\Phi_d: \mathbb{R}^N \rightarrow (0, 1)^N$  returns the elementwise application of the function

$$\phi_d(x) = \frac{d}{dx} \phi(x) = \frac{1}{1 + e^{-x}}.$$

**Theorem 2.1: (Parametrization using  $d$ )** For any matrix  $W \in \mathbb{R}^{N \times N}$  and vector  $\bar{d} \in (0, 1)^N$ , there exists  $x_{\text{eq}}$  and  $d$  that satisfy equation (2) and  $\Phi_d(Wx_{\text{eq}} + d) = \bar{d}$ .

*Proof:* Notice that  $\phi_d$  is a injective function, so that its inverse is well defined. Let  $x_{\text{eq}} = \Phi[\Phi_d^{-1}(\bar{d})]$  and  $d = \Phi_d^{-1}(\bar{d}) - W\Phi[\Phi_d^{-1}(\bar{d})]$ . Then, from (2),

$$\begin{aligned} x_{\text{eq}} &= \Phi(W\Phi[\Phi_d^{-1}(\bar{d})] + \Phi_d^{-1}(\bar{d}) - W\Phi[\Phi_d^{-1}(\bar{d})]) \\ &= \Phi(\Phi_d^{-1}(\bar{d})) = x_{\text{eq}}. \end{aligned}$$

Further, to conclude,

$$\Phi_d(W\Phi[\Phi_d^{-1}(\bar{d})] + \Phi_d^{-1}(\bar{d}) - W\Phi[\Phi_d^{-1}(\bar{d})]) = \bar{d}. \quad \blacksquare$$

Theorem 2.1 shows that there exists a vector  $d$  and an equilibrium  $x_{\text{eq}}$  that realizes any desired matrix  $D$  in (3). Hence, in what follows, we derive conditions and algorithms for the matrix  $D$ , with the understanding that such matrix can ultimately be realized by choosing the vector  $d$ . Now we are ready to formally state our multi-task control problem, consider a set of  $M$  distinct, stable, controllable, and observable linear, time-invariant systems denoted as

$$\Sigma_i^D = (A_i, B_i, C_i), \quad (4)$$

with  $A_i \in \mathbb{R}^{n \times n}$ ,  $B_i \in \mathbb{R}^{n \times m}$ ,  $C_i \in \mathbb{R}^{p \times n}$  and  $i = 1, \dots, M$ . Our multi-task control problem is

$$\min_{W, D_1, \dots, D_M, B, C} \sum_{i=1}^M \|\Sigma_i^D - \Sigma_i^L\|_2^2, \quad (5)$$

where  $\Sigma_i^L$  denotes the  $i$ -th linearized dynamics (3) with diagonal matrix  $D_i$  and  $\|\cdot\|_2$  the  $\mathcal{H}_2$ -norm.

*Remark 1:* Problem (5) is treated as an optimal approximation problem rather than a traditional control problem, since the focus of this paper is on the approximation capabilities of the biologically inspired non-linear neural controller (1), rather than the control performance of the systems  $\Sigma_i^D$ , which may represent LQR controllers or general systems. We also note that the implementation of a neural controller may be more efficient than the separate implementation of multiple controllers. In fact, storing  $M$  distinct linear controllers as in (4) requires  $Mn^4mp$  parameters that define the matrices  $A_i$ ,  $B_i$ , and  $C_i$ . In contrast, the neural controller (1) only needs  $MN + N^4mp$  parameters, making it more efficient as  $M$  increases and  $N < n^4mp$ .  $\square$

*Remark 2:* Although Problem (5) is formulated under the assumption that all systems in the set (4) share the same state dimension  $n$ , this simplification is made primarily for the ease of notation. The theoretical derivations, including the gradient computations discussed in Section III, are easily adaptable to scenarios where the systems  $\Sigma_i^D$  have distinct state dimensions  $n_i$ .  $\square$

In the minimization problem (5), the optimization variables allow the neural controller (1) to approximate the desired systems (4) locally around its equilibrium points. The approximation error in (5) depends in a nontrivial way on several parameters, including the dimension of the neural controller, the number, and the diversity of the systems to be approximated. In the following sections, we define both upper and lower bounds on the approximation error, as detailed in Section IV. Furthermore, in Section III, we derive the gradient useful to implement a numerical procedure based on a gradient descent to solve the minimization problem (5).

### III. GRADIENT-BASED MULTI-TASK CONTROL

This section contains the analytical expression of the gradient of the multi-task control problem (5) with respect to the matrices of the neural controller. These expressions can be used to numerically optimize the performance of the neural controller given a set of desired control tasks. To this aim, define the following error system and matrices:

$$\Sigma_{\text{err}}^i = (A_{\text{err}}^i, B_{\text{err}}^i, C_{\text{err}}^i),$$

with

$$A_{\text{err}}^i = \begin{bmatrix} A_i & 0 \\ 0 & -I + D_i W \end{bmatrix}, \quad B_{\text{err}}^i = \begin{bmatrix} B_i \\ B \end{bmatrix}, \\ C_{\text{err}}^i = [C_i \quad -C],$$

and observability ( $Q^i$ ) and controllability ( $P^i$ ) Gramians as

$$Q^i = \begin{bmatrix} Q_{11}^i & Q_{12}^i \\ Q_{12}^{i\top} & Q_{22}^i \end{bmatrix}, \quad P^i = \begin{bmatrix} P_{11}^i & P_{12}^i \\ P_{12}^{i\top} & P_{22}^i \end{bmatrix}.$$

**Theorem 3.1: (Analytical gradient of (5))** The gradient of the minimization problem (5) is as follows:

$$\frac{\partial \mathcal{J}}{\partial W} = 2 \sum_{i=1}^M D_i \left( Q_{12}^{i\top} P_{12}^i + Q_{22}^i P_{22}^i \right), \\ \frac{\partial \mathcal{J}}{\partial B} = 2 \sum_{i=1}^M \left( Q_{12}^{i\top} B_i + Q_{22}^i B \right), \\ \frac{\partial \mathcal{J}}{\partial C} = 2 \sum_{i=1}^M \left( -C_i P_{12}^i + C P_{22}^i \right), \\ \frac{\partial \mathcal{J}}{\partial (D_i)_{hh}} = 2 \left( \left( Q_{12}^{i\top} P_{12}^i + Q_{22}^i P_{22}^i \right) W^\top \right)_{hh}. \quad (6)$$

*Proof:* Let

$$\mathcal{J}_i = \|\Sigma_i^D - \Sigma_i^L\|_2^2 \quad i = 1, \dots, M,$$

and notice from [26] that

$$\frac{\partial \mathcal{J}_i}{\partial A_{\text{err}}^i} = \frac{\partial \|\Sigma_{\text{err}}^i\|_2^2}{\partial A_{\text{err}}^i} = 2Q^i P^i.$$

Using the chain rule [27] we obtain

$$\frac{\partial \mathcal{J}_i}{\partial (W)_{hl}} = \sum_{k=1}^{N+n} \sum_{j=1}^{N+n} \frac{\partial \mathcal{J}_i}{\partial (A_{\text{err}}^i)_{kj}} \frac{\partial (A_{\text{err}}^i)_{kj}}{\partial (W)_{hl}} \\ = \frac{\partial \mathcal{J}_i}{\partial (A_{\text{err}}^i)_{(n+h)(n+l)}} \frac{\partial (A_{\text{err}}^i)_{(n+h)(n+l)}}{\partial (W)_{hl}} \quad (7) \\ = 2(D_i)_{hh} (Q_i P_i)_{(n+h)(n+l)},$$

where we have used the fact that, for any  $1 \leq h \leq N$  and  $1 \leq l \leq N$ , it holds

$$\frac{\partial (A_{\text{err}}^i)_{kj}}{\partial w_{hl}} = \begin{cases} (D_i)_{hh} & \text{if } (k, j) = (n+h, n+l) \\ 0 & \text{otherwise} \end{cases}.$$

Rewriting (7) in compact matrix form and summing over the index  $i$  we obtain the first equation in (6). With a similar reasoning we obtain

$$\frac{\partial (A_{\text{err}}^i)_{kj}}{\partial (D_i)_{hh}} = \begin{cases} w_{h(j-n)} & \text{if } k = n+h \wedge n < j \leq n+N \\ 0 & \text{otherwise} \end{cases}$$

and, for any  $i = 1, \dots, M$ ,

$$\frac{\partial \mathcal{J}}{\partial (D_i)_{hh}} = \frac{\partial \mathcal{J}_i}{\partial (D_i)_{hh}} = 2 \left( Q^i P^i \begin{bmatrix} 0 & 0 \\ 0 & W^\top \end{bmatrix} \right)_{(n+h)(n+h)}.$$

This leads to the last equation of (6).

The derivation of  $\frac{\partial \mathcal{J}}{\partial C}$  and  $\frac{\partial \mathcal{J}}{\partial B}$  is different. Recall that

$$\|\Sigma_{\text{err}}^i\|_2^2 = \text{tr} \left( C_{\text{err}}^i P^i C_{\text{err}}^{i\top} \right) = \text{tr} \left( B_{\text{err}}^{i\top} Q^i B_{\text{err}}^i \right).$$

Notice that  $\frac{\partial \mathcal{J}_i}{\partial B_{\text{err}}^i} = 2Q^i B_{\text{err}}^i$ , and that

$$\frac{\partial \mathcal{J}_i}{\partial (B)_{hl}} = \sum_{k=1}^{N+n} \sum_{j=1}^m \frac{\partial \mathcal{J}_i}{\partial (B_{\text{err}}^i)_{kj}} \frac{\partial (B_{\text{err}}^i)_{kj}}{\partial (B)_{hl}} \\ = \frac{\partial \mathcal{J}_i}{\partial (B_{\text{err}}^i)_{(n+h)l}} = 2 \left( Q^i B_{\text{err}}^i \right)_{(n+h)l}.$$

Equivalently in compact form, we have

$$\frac{\partial \mathcal{J}_i}{\partial B} = 2 \left( Q_{12}^{i \top} B_i + Q_{22}^i B \right), \quad (8)$$

and, with a similar procedure,

$$\frac{\partial \mathcal{J}_i}{\partial C} = 2 \left( -C_i P_{12}^i + C P_{22}^i \right). \quad (9)$$

To conclude, summing over  $i = 1, \dots, M$  on (8) and (9) we get the remaining two equations of (6). ■

The gradient in Theorem (3.1) allows us to use gradient descent methods to approximate a solution to the minimization problem (5). We conclude this section with an example.

Consider the systems in Fig. 1 with simplified dynamics

$$\begin{aligned} \Sigma_{\text{Aircraft}} &= \left( \begin{bmatrix} 0 & 0 \\ 0 & 0 \end{bmatrix}, \begin{bmatrix} 0 \\ r/J \end{bmatrix}, [0 \quad 1] \right), \\ \Sigma_{\text{Pendulum}} &= \left( \begin{bmatrix} 0 & 1 \\ \frac{mgl}{J_t} & 0 \end{bmatrix}, \begin{bmatrix} 0 \\ \frac{1}{J_t} \end{bmatrix}, [1 \quad 0] \right), \\ \Sigma_{\text{Pendulum + frict.}} &= \left( \begin{bmatrix} 0 & 1 \\ \frac{mgl}{J_t} & \frac{\gamma}{J_t} \end{bmatrix}, \begin{bmatrix} 0 \\ \frac{1}{J_t} \end{bmatrix}, [1 \quad 0] \right), \\ \Sigma_{\text{Bicycle}} &= \left( \begin{bmatrix} 0 & 1 \\ \frac{mgh}{J} & 0 \end{bmatrix}, \begin{bmatrix} \frac{Dv_0}{bJ} \\ \frac{mv_0^2 h}{bJ} \end{bmatrix}, [1 \quad 0] \right). \end{aligned} \quad (10)$$

Let  $g = 9.8$  and other specific parameters as in [28]:

$J_p$	$m$	$l$	$\gamma$	$J$	$r$
0.006	0.2	0.3	0.01	0.0475	25

$D$	$v_0$	$M$	$h$	$b$	$J_b$
4.8	2.5	8	1	1.2	8

The systems  $\Sigma_i^D$ , with  $i = 1, \dots, 4$ , to be approximated with the neural controller, of dimension  $N = 3$ , are the Linear Quadratic Regulators of the systems (10), with identity cost matrices. Fig. 2 shows the impulse responses of the desired systems  $\Sigma_i^D$  and the neural controller, which is optimized using the gradient in Theorem 3.1. While this numerical gradient-based procedure offers no stability or performance guarantees (see Section IV for some fundamental performance limitations of our approach), our numerical studies show promising results and demonstrate the viability of our multi-task control approach. An additional observation supporting this fact comes from the simulation results depicted in Fig. 3. Here, we consider  $M = 5$  randomly generated SISO systems ( $n = 2$ ) and we show the evolution of the cost (5) as the dimension  $N$  of the neural controller increases. Notably, even for small values of  $N$ , the neural controller exhibits significant approximation capabilities.

In our final numerical example, we explore a scenario involving randomly generated SISO systems ( $n = 2$ ) and neural controllers of dimension  $N = 4$ . Fig. 4 demonstrates how the cost (5) evolves as the number of systems increases.

#### IV. BOUNDS ON MULTI-TASK CONTROL PROBLEM

In this section we establish upper and lower bounds for the optimization problem (5), as a function of the number and properties of the systems to be approximated.

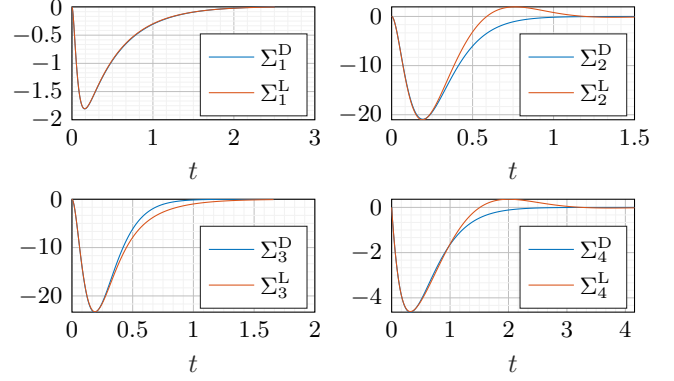


Fig. 2. This figure displays the impulse responses of the feedback interconnection between the desired controllers  $\Sigma_i^D$  (or their implementations via the neural controller (1)) and the plants described in Fig. 1. The closed-loop impulse responses associated with the approximating controllers, which are the result of linearizing our neural controller, are highlighted in red. In contrast, the impulse responses of the closed-loop systems governed by the desired controllers are illustrated in blue.

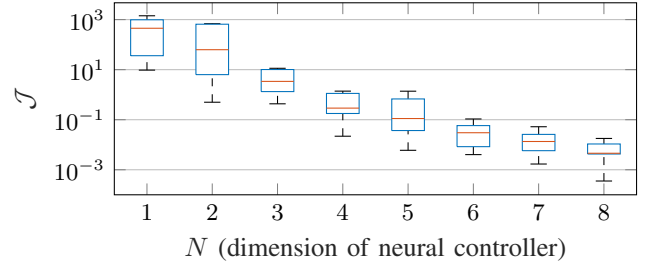


Fig. 3. This figure illustrates a box plot summarizing the final cost (5) across 17 simulations with distinct sets ( $M = 5$ ) of randomly generated systems  $\Sigma_i^D$ , as the dimension  $N$  of the neural controller increases from 1 to 8. The median of the simulations is marked by the central red line in each box, while the bottom and top edges of the box delineate the 25<sup>th</sup> and 75<sup>th</sup> percentiles, respectively. The whiskers extend to cover approximately 99.3% of the data, indicating the range within which most observations lie.

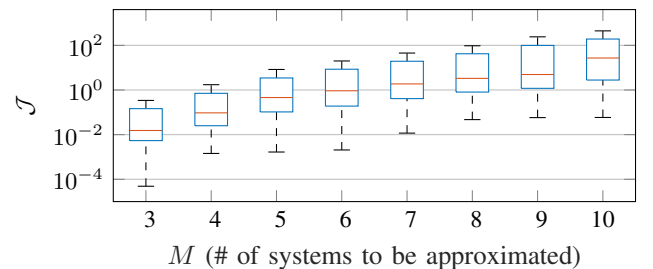


Fig. 4. This figure shows a box plot (with the format introduced in Fig. 3) aggregating the final cost (5) across 100 simulations for 100 randomly selected sets of  $\Sigma_i^D$ . For each set, we calculate the cost (5), considering increasing subsets of systems to be approximated, with the number of systems  $M$  increasing from 3 to 10.

### A. Upper bound

To derive an upper bound, we notice that the approximation error in (5) obtained when choosing  $M$  different matrices  $D_i$  is certainly bounded above by the error incurred when such  $D_i$  matrices are all equal to each other. That is, solving the following minimization problem provides an upper bound on the solution to the minimization problem (5):

$$\min_{W,D,B,C} \sum_{i=1}^M \|\Sigma_i^D - \Sigma^L\|_2^2. \quad (11)$$

The minimization problem (11) is akin to a model reduction problem to approximate a given set of systems.

We start by introducing the necessary notation and preliminary steps to present our result. Define the parallel system

$$\Sigma_{\text{ext}} = (A_{\text{ext}}, B_{\text{ext}}, C_{\text{ext}}), \quad (12)$$

with

$$A_{\text{ext}} = \begin{bmatrix} A_1 & & \\ & \ddots & \\ & & A_M \end{bmatrix}, B_{\text{ext}} = \begin{bmatrix} B_1 \\ \vdots \\ B_M \end{bmatrix},$$

$$C_{\text{ext}} = \begin{bmatrix} C_1 & & \\ & \ddots & \\ & & C_M \end{bmatrix},$$

and its balanced and minimal realization [29]

$$\Sigma_{\text{ext}}^B = (A_{\text{ext}}^B, B_{\text{ext}}^B, C_{\text{ext}}^B), \quad (13)$$

with

$$A_{\text{ext}}^B = \begin{bmatrix} A_{\text{ext}11}^B & A_{\text{ext}12}^B \\ A_{\text{ext}21}^B & A_{\text{ext}22}^B \end{bmatrix}, B_{\text{ext}}^B = \begin{bmatrix} B_{\text{ext}1}^B \\ B_{\text{ext}2}^B \end{bmatrix}, \quad (14)$$

$$C_{\text{ext}}^B = \begin{bmatrix} C_{\text{ext}1}^B & C_{\text{ext}2}^B \end{bmatrix}.$$

Notice that the dimension of  $\Sigma_{\text{ext}}^B$  is potentially smaller than the dimension of  $\Sigma_{\text{ext}}$  since the latter may not be a minimal realization. Let  $R$  be the dimension of  $\Sigma_{\text{ext}}^B$  and let  $N$  be the dimension of the sub block  $A_{\text{ext}11}^B$  when  $R > N$ .<sup>1</sup> Then, the controllability Gramian  $P_{\text{ext}}^B$  and observability Gramian  $Q_{\text{ext}}^B$  of (13) are diagonal and equal to each other:

$$P_{\text{ext}}^B = Q_{\text{ext}}^B = \begin{bmatrix} S_1 & \\ & S_2 \end{bmatrix} > 0, \quad (15)$$

with  $S_1 = \text{diag}(\sigma_1, \dots, \sigma_N)$ ,  $S_2 = \text{diag}(\sigma_{N+1}, \dots, \sigma_R)$ , and  $\sigma_i$  Hankel singular value of the system (13) [30].

**Theorem 4.1: (Upper bound of (5))** Let  $\Sigma_1^L, \dots, \Sigma_M^L$  and  $\Sigma_1^D, \dots, \Sigma_M^D$  be the LTI systems defined in equations (3) and (4), respectively. Then if  $R > N$ :

$$\min_{W,D,B,C} \sum_{i=1}^M \|\Sigma_i^D - \Sigma_i^L\|_2^2 \leq (\mathcal{J}^B + \sqrt{\sigma_1} \|\Delta C\|_F)^2, \quad (16)$$

if  $R \leq N$

$$\min_{W,D,B,C} \sum_{i=1}^M \|\Sigma_i^D - \Sigma_i^L\|_2^2 \leq \sigma_1 \|\Delta C\|_F^2, \quad (17)$$

<sup>1</sup>If  $R \leq N$  we let  $A_{\text{ext}}^B = A_{\text{ext}11}^B$ ,  $B_{\text{ext}}^B = B_{\text{ext}1}^B$  and  $C_{\text{ext}}^B = C_{\text{ext}1}^B$ .

and where, using the notation in (14),<sup>2</sup>

$$\mathcal{J}^B = \sqrt{\text{tr} \left[ B_{\text{ext}2}^B \top S_2 B_{\text{ext}2}^B \right] + 2N \|\Sigma_{\text{aux}}\|_\infty},$$

with  $\Sigma_{\text{aux}} = (A_{\text{ext}}^B, B_{\text{aux}}, C_{\text{aux}})$ ,

$$B_{\text{aux}} = \begin{bmatrix} 0 \\ S_2 A_{\text{ext}21}^B \end{bmatrix}, C_{\text{aux}} = \begin{bmatrix} 0 & A_{\text{ext}12}^B S_2 \end{bmatrix},$$

and

$$\Delta C = \left( I - \frac{1}{M} \begin{bmatrix} I \\ \vdots \\ I \end{bmatrix} \begin{bmatrix} I & \cdots & I \end{bmatrix} \right) C_{\text{ext}1}^B.$$

Some comments are in order to fully appreciate the result in Theorem 4.1. First,  $R > N$  when the dimension of the neural controller is smaller than the number of different modes to be approximated (as found through the balanced realization of (12)). Similarly,  $R \leq N$  when the neural controller is larger than the number of different modes of the systems to be approximated. Second, the term  $\mathcal{J}^B$  in (16) depends on the Hankel singular values that the neural controller is not able to approximate ( $S_2$  in (15)). This term vanishes when the dimension of the neural controller is sufficiently large to capture all the modes of the systems to be approximated (as in (17)). As similar error is also done when using the balanced truncation technique to obtain a reduced dynamical model [30]. Third, the error  $\Delta C$  in (16) and (17) is due to the fact that the system (13) to be approximated has more outputs than the neural controller. To minimize such discrepancy and compute an upper bound on the approximation error, Theorem 4.1 uses the average of the rows of the desired output matrix (namely,  $\frac{1}{M} [I \ \cdots \ I] C_{\text{ext}1}^B$ , which minimizes the discrepancy of the output matrices as measured by the Frobenius norm). In the special case when the systems to be approximated are all equal to each other, such error vanishes as the average of the output matrices equals the actual output matrices. Similarly, this error becomes small when the output matrices in the balanced realization of the systems to be approximated are similar across the systems to be approximated. Thus, Theorem 4.1 shows that the multi-task control approximation error depends on (i) the order of the neural controller through  $\mathcal{J}^B$ , which dictates the number of different modes that can be approximated, and (ii) the similarity of the systems to be approximated through  $\Delta C$ . We are now ready to formally prove Theorem 4.1.

*Proof:* We derive the proof separately for two cases  $R > N$  and  $R \leq N$ .

( $R > N$ ) We use the minimization problem (11) as an upper bound for the minimization problem (5), and we compute the solution to (11) by using the  $N$  dominant modes of the balanced realization (13). In particular, select  $W$ ,  $D$ , and  $B$  in (11) such that  $-I + DW = A_{\text{ext}11}^B$  and  $B = B_{\text{ext}1}^B$ ,

<sup>2</sup>We use  $\|\cdot\|_F$  and  $\|\cdot\|_\infty$  to denote the Frobenius and the  $\mathcal{H}_\infty$  norms.

and  $C = \frac{1}{M} [I \ \cdots \ I] C_{\text{ext}1}^{\text{B}}$ .<sup>3</sup> Then, the cost in (11) becomes

$$\sum_{i=1}^M \|\Sigma_i^{\text{D}} - \Sigma^{\text{L}}\|_2^2 = \|\Sigma_{\text{ext}} - \Sigma_{\text{ext}}^{\text{L}}\|_2^2,$$

where

$$\Sigma_{\text{ext}}^{\text{L}} = \begin{pmatrix} A_{\text{ext}11}^{\text{B}}, B_{\text{ext}1}^{\text{B}}, \underbrace{\begin{bmatrix} C \\ \vdots \\ C \end{bmatrix}}_{C_{\text{ext}}^{\text{L}}} \end{pmatrix}.$$

Let  $\Delta C = C_{\text{ext}1}^{\text{B}} - C_{\text{ext}}^{\text{L}}$  and notice that

$$\|\Sigma_{\text{ext}} - \Sigma_{\text{ext}}^{\text{L}}\|_2^2 \leq (\|\Sigma_{\text{ext}} - \Sigma_{\text{ext}1}\|_2 + \|\Sigma_{\text{err}}\|_2)^2, \quad (18)$$

where  $\Sigma_{\text{ext}1} = (A_{\text{ext}11}^{\text{B}}, B_{\text{ext}1}^{\text{B}}, C_{\text{ext}1}^{\text{B}})$  and

$$\Sigma_{\text{err}} = (A_{\text{ext}11}^{\text{B}}, B_{\text{ext}1}^{\text{B}}, \Delta C).$$

Notice that

$$\|\Sigma_{\text{err}}\|_2^2 = \text{tr}(S_1 \Delta C^{\text{T}} \Delta C) \leq \sigma_1 \|\Delta C\|_F^2,$$

where  $S_1$  and  $\sigma_1$  are as in (15). In summary, leveraging the upper bound on the balanced truncation presented in [30], inequality (18) yields

$$\|\Sigma_{\text{ext}} - \Sigma_{\text{ext}}^{\text{L}}\|_2^2 \leq (\mathcal{J}^{\text{B}} + \sqrt{\sigma_1} \|\Delta C\|_F)^2.$$

( $R \leq N$ ) The balance realization (14) is already of order less than  $N$  and represents a minimal realization of realization (12). For this reason choosing

$$\begin{aligned} -I + DW &= \begin{bmatrix} A_{\text{ext}}^{\text{B}} & 0 \\ 0 & -I \end{bmatrix} & B &= \begin{bmatrix} B_{\text{ext}}^{\text{B}} \\ 0 \end{bmatrix} \\ C &= \left[ \frac{1}{M} [I \ \cdots \ I] C_{\text{ext}}^{\text{B}} \ 0 \right], \end{aligned}$$

the first term in (18) is zero and then we obtain (17). ■

To conclude, we provide an example to evaluate the upper bound in Theorem 4.1. Using the dataset utilized for Fig. 4, Fig. 5 illustrates the curves of the upper bound delineated in Theorem 4.1 and the error incurred by the neural controller obtained using the gradient in Section III (both curves are plotted by averaging the results over the same 100 experiments as demonstrated in Fig. 4).

### B. Lower bounds

Computing a lower bound for the multi-task control problem (5) presents considerable challenges, as the existing model reduction tools cannot be applied in a straightforward way. In this section we consider two alternative formulations of the minimization problem (5), which capture the fundamental limitations of multi-task control problems, although using different performance metrics than in (5). In particular,

<sup>3</sup>The output matrix  $C$  of the neural controller have different dimensions than  $C_{\text{ext}1}^{\text{B}}$ , which prevents us from implementing the balanced truncation method to find the controller that minimize the cost (11).

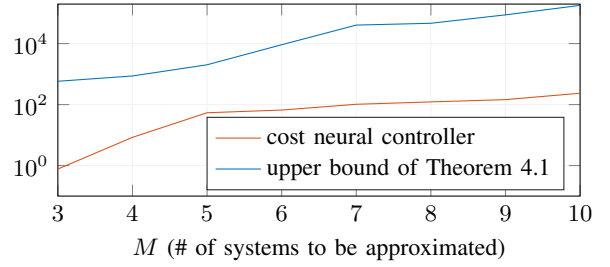


Fig. 5. The figure illustrates two distinct curves: the red one represents the evolution of the minimum of the cost function (5) derived via a gradient descent algorithm that utilizes the gradient discussed in Section III; the blue curve shows the upper bound (16). These outcomes are averaged across the same 100 simulations of Fig. 4.

we consider the following multi-task control minimization problems:

$$\min_{W, D_1, \dots, D_M, B, C} \underbrace{\sum_{i=1}^M \sup_{t \geq 0} \|g_i^{\text{D}}(t) - g_i^{\text{L}}(t)\|_2}_{\mathcal{J}_2}, \quad (19)$$

and

$$\inf_{W, D_1, \dots, D_M, B, C} \underbrace{\sum_{i=1}^M \|\Sigma_i^{\text{D}} - \Sigma_i^{\text{L}}\|_1}_{\mathcal{J}_1}. \quad (20)$$

In (19)  $\|\cdot\|_2$  denotes the 2-induced matrix norm, with  $g_i^{\text{D}}(t)$  and  $g_i^{\text{L}}(t)$  representing the impulse responses of  $\Sigma_i^{\text{D}}$  and  $\Sigma_i^{\text{L}}$ , respectively. For this problem we provide a simple lower bound, which may be conservative in some cases. Instead, in (20),  $\|\cdot\|_1$  denotes the 1-norm of the impulse response of the system and it can be interpreted as the induced norm of the system for signals of bounded magnitude. We will solve this problem exactly, but only for a class of scalar systems. We now proceed with a lower bound for (19).

**Theorem 4.2: (Lower bound of (19))** Using the notation in (3) and (4), we have

$$\min_{W, D_1, \dots, D_M, B, C} \mathcal{J}_2 \geq \sqrt{\frac{\sum_{i=1}^M \|C_i B_i - (\sum_{i=1}^M C_i B_i) / M\|_F^2}{\min\{p, m\}}}. \quad (21)$$

Theorem 4.2 provides a bound for the minimization problem (19) by substituting the supremum over time with the evaluation of the impulse response at time zero. When doing so, the error only depends on the input and output matrices, and it is minimized by choosing the input and output matrices of the neural controller as the average of the input and output matrices of the systems to be approximated. Clearly, this can result in a conservative bound. We now prove Theorem 4.2.

*Proof:* We start our discussion by stating:

$$\min_{W, D_1, \dots, D_M, B, C} \mathcal{J}_2 \geq \min_{X_1, \dots, X_M, B, C} \underbrace{\sum_{i=1}^M \sup_{t \geq 0} \|g_i^{\text{D}}(t) - \hat{g}_i^{\text{L}}(t)\|_2}_{\tilde{\mathcal{J}}_2} \quad (22)$$

where  $\widehat{g}_i^L$  denotes the impulse response of systems  $\widehat{\Sigma}_i^L$  defined as:

$$\widehat{\Sigma}_i^L = (X_i, B, C),$$

where we assume  $X_i \in \mathbb{R}^{N \times N}$  for each index  $i = 1, \dots, M$ . This formulation of the problem acts as a lower bound to (5) since the set of optimization variables in (22) encapsulates all optimization variables considered in (5). Moreover, by setting  $CB = \left( \sum_{i=1}^M C_i B_i \right) / M$ , we obtain (21). Indeed,

$$\begin{aligned} \widehat{\mathcal{J}}_2 &= \sum_{i=1}^M \sup_{t \geq 0} \|C_i e^{A_i t} B_i - C e^{X_i t} B\|_2 \quad (23) \\ &\geq \sum_{i=1}^M \|C_i B_i - CB\|_2 \geq \sum_{i=1}^M \sqrt{\|C_i B_i - CB\|_2^2} \\ &\geq \sqrt{\sum_{i=1}^M \|C_i B_i - CB\|_2^2} \geq \sqrt{\frac{\sum_{i=1}^M \|C_i B_i - CB\|_F^2}{\min\{p, m\}}}, \end{aligned}$$

where the final inequality in equation (23) derives from the fact that for any  $X \in \mathbb{R}^{p \times m}$  we have  $\|X\|_2 \geq \frac{1}{\sqrt{d}} \|X\|_F$ , where  $d$  is the rank of matrix  $X$  [27]. Then, minimizing last term (23) with respect to  $CB$  gives (21). ■

We now present our last lower bound, which is valid for a special class of stable single input, single output systems.

**Theorem 4.3: (Lower bound of (20))** Let  $\Sigma_i^D = (a_i, b_i, c_i)$  satisfy  $a_i < 0$  and  $r_i = b_i c_i > 0$  for all  $i = 1, \dots, M$ . Let, without loss of generality,  $r_1 \leq r_2 \leq \dots \leq r_M$ . Let  $\Sigma_i^L$  as in (3) with  $N = 1$ . Define the function

$$A(j, l) = \frac{r_j}{a_j} - \frac{r_l}{a_j} \left( \frac{\ln(r_l/r_j)}{W_{-1}(-1/2e)} + 1 \right),$$

valid for any pair of indices  $1 \leq j < l \leq M$ , where  $W_{-1}(\cdot)$  denotes the W Lambert function on the negative branch [31]. Then,

$$\inf_{\substack{W, D_1, \dots, D_M \\ B, C}} \mathcal{J}_1 \geq \min \left\{ A(j, l), -A(l, j), -\frac{r_j}{a_j} \right\}. \quad (24)$$

Some comments are in order. First, when  $M = 2$ , the bound in (24) holds with equality, thus providing an optimal solution to (20). In this case, it can be shown that the optimal solution requires the neural controller to satisfy  $\|\Sigma_1^D - \Sigma_1^L\|_1 = 0$  or  $\|\Sigma_2^D - \Sigma_2^L\|_1 = 0$ , that is, to equal one of the two systems to be approximated. Second, when  $M > 2$ , the bound is obtained by selecting only two of the systems to be approximated. Thus, the bound (24) can be sharpened by maximizing over the indices  $i$  and  $j$  that correspond to the selected systems. We now prove Theorem 4.3.

*Proof:* For any pair of indices  $1 \leq j < l \leq M$ , it holds that:

$$\inf_{\substack{W, D_1, \dots, D_M \\ B, C}} \mathcal{J}_1 \geq \underbrace{\inf_{\substack{W, D_j, D_l \\ B, C}} \left( \|\Sigma_j^D - \Sigma_j^L\|_1 + \|\Sigma_l^D - \Sigma_l^L\|_1 \right)}_{\widetilde{\mathcal{J}}_1}. \quad (25)$$

Because  $N = 1$  we can define the scalar quantities  $r = BC$ ,  $x_l = -1 + D_l W$  and  $x_j = -1 + D_j W$  and noticing that (25)

is equivalent to minimize over  $r$ ,  $x_j$  and  $x_l$ , we will show that the optimal value of the right-hand side of (25) are realized for:

	Case 1	Case 2	Case 3
$r$	$r_j$	$r_l$	$r_l$
$x_l$	$x_l^*(r_j)$	$a_l$	$a_l$
$x_j$	$a_j$	$x_j^*(r_l)$	$-\infty$

(26)

where each case corresponds to a unique term within the minimum argument of inequality (24), with

$$x_j^*(r) = \begin{cases} a_j \frac{y_j^*(r)}{y_j^*(r)+1} & \text{if } r > r_j \\ a_j & \text{if } r = r_j \end{cases} \quad (27)$$

$$x_l^*(r) = \begin{cases} a_l \frac{y_l^*(r)}{y_l^*(r)-1} & \text{if } r < r_l \\ a_l & \text{if } r = r_l \end{cases}, \quad (28)$$

and

$$y_j^*(r) = \ln(r/r_j)^{-1} [1 + W_{-1}(-1/2e)] \quad (29)$$

$$y_l^*(r) = \ln(r_l/r)^{-1} [1 + W_{-1}(-1/2e)]. \quad (30)$$

To prove (26) we first fix  $r_j \leq r \leq r_l$  and minimize over  $x_j(r)$  and  $x_l(r)$ , secondly we optimize the solution over  $r$ . The proofs for the conditions  $r \leq r_j$  and  $r \geq r_l$  are not included, as they lead to analogous conclusions through similar arguments. If  $x_j > a_j$  and  $x_l < a_l$  it is possible to establish that the minimum of  $\widetilde{\mathcal{J}}_1$  with  $r$  fixed is achieved as  $x_j \rightarrow a_j^+$  and  $x_l \rightarrow a_l^-$ . So we proceed assuming  $x_j \leq a_j$  and  $x_l \geq a_l$ . In particular, if  $x_j < a_j$  and  $x_l > a_l$ , there will be a point where the impulse responses of  $\Sigma_j^L$  and  $\Sigma_j^D$ , as well as  $\Sigma_l^L$  and  $\Sigma_l^D$ , intersect. Applying the following changes of variable

$$\begin{aligned} y_j: (-\infty, a_j) &\longrightarrow (-\infty, -1) \\ x_j &\longmapsto \frac{x_j}{a_j - x_j} \\ y_l: (a_l, 0) &\longrightarrow (-\infty, 0) \\ x_l &\longmapsto \frac{x_l}{x_l - a_l}. \end{aligned}$$

to  $\widetilde{\mathcal{J}}_1 = \widetilde{A}_j + \widetilde{A}^l$  yields:

$$\widetilde{A}_j(y_j, r) = \frac{r(2e^{y_j \ln(r/r_j)} - 1)}{a_j y_j} - \frac{r}{a_j} + \frac{r_j}{a_j} \quad (31)$$

$$\widetilde{A}^l(y_l, r) = \frac{r(2e^{y_l \ln(r_l/r)} - 1)}{a_l y_l} + \frac{r}{a_l} - \frac{r_l}{a_l}.$$

Computing  $\frac{\partial}{\partial y_j} \widetilde{A}_j(y_j, r) = 0$  we derive the following equation:

$$2 \ln(r/r_j) e^{y_j \ln(r/r_j)} - 2e^{y_j \ln(r/r_j)} + 1 = 0. \quad (32)$$

This transcendental equation, solvable via the Lambert W function  $W_{-1}(\cdot)$  yields only one negative solution (29) for  $j$ , and similarly (30) for  $l$ . Finally, one can observe that they are also actual minima within  $y_j$  and  $y_l$  in the interval  $(-\infty, 0)$ . For (31) we have to distinguish two scenarios depending on the value of  $r$  in  $r_j \leq r \leq r_l$ :

- $y_j^* \in (-\infty, -1)$  if  $r < r_j e^{-[1+W_{-1}(-1/2e)]}$ ;
- $y_j^* \notin (-\infty, -1)$  if  $r \geq r_j e^{-[1+W_{-1}(-1/2e)]}$ .

In particular if  $r_l < r_j e^{-[1+W_{-1}(-1/2e)]}$ , then we are definitely in Scenario a, and it is possible to prove that  $\tilde{\mathcal{J}}_1$  in the interval  $r_j < r < r_l$ , with  $x_j = x_j^*(r)$ ,  $x_l = x_l^*(r)$ , as in (27) and (28), admits no local minimum in  $r$ . Therefore, according to the Weierstrass Extreme Value Theorem, the minimum for  $r_j \leq r \leq r_l$  must be located at the boundaries of the given interval. Resulting in

$$\min \left\{ \tilde{A}^l(x_l^*(r_j), r_j), \tilde{A}_j(x_j^*(r_l), r_l) \right\} = \inf_{x_j, x_l, r} \tilde{\mathcal{J}}_1, \quad (33)$$

and falling back to Cases 1 and 2 in the table (26).

Conversely, in Scenario b, when  $r_j e^{-[1+W_{-1}(-1/2e)]} \leq r \leq r_l$ , for reasons of monotonicity it can be shown that:

$$\tilde{A}_j(x_j, r) \xrightarrow{x_j \rightarrow -\infty} -\frac{r_j}{a_j} = \inf_{x_j} \tilde{A}_j(x_j, r).$$

Since this last infimum is independent of  $x_l$  and  $r$ , we find

$$\inf_{x_j, x_l, r} \tilde{\mathcal{J}}_1 \geq -\frac{r_j}{a_j} + \underbrace{\inf_{x_l, r} \tilde{A}^l(x_l, r)}_{=0}.$$

This inequality is then related to the parameters defined in Case 3 of Table (26).

For  $r_j \leq r < r_j e^{-[1+W_{-1}(-1/2e)]}$ , we can proceed as before, leading to

$$\inf_{x_j, x_l, r} \tilde{\mathcal{J}}_1 = \inf_{W, D_j, D_l, B, C} \tilde{\mathcal{J}}_1 \geq \min \left\{ \tilde{A}^l(x_l^*(r_j), r_j), -\frac{r_j}{a_j} \right\}. \quad (34)$$

Combining the minima from (33) and (34), we obtain the relationship (24), where  $\tilde{A}^l(x_l^*(r_j), r_j) = -A(l, j)$  and  $\tilde{A}_j(x_j^*(r_l), r_l) = A(j, l)$ . ■

## V. CONCLUSION AND FUTURE WORK

This paper addresses the problem of approximating multiple linear systems using a single non-linear neural controller. Key contributions of this work include a characterization of the approximation performance of the neural controller, in terms of analytical lower and upper bounds, and the design of gradient-based algorithms to train the controller parameters. Directions of future work include the design of switching mechanisms to engage different controller modalities, as well a study of the approximation properties of the neural controller away from the pre-specified systems.

## REFERENCES

- [1] J. Baxter, "A model of inductive bias learning," *Journal of Artificial Intelligence Research*, vol. 12, pp. 149–198, 2000.
- [2] R. Caruana, "Multitask learning," *Machine Learning*, vol. 28, no. 1, p. 41, 1997.
- [3] L. Gong, F. Pasqualetti, T. Papouin, and S. Ching, "Astrocytes as a mechanism for meta-plasticity and contextually-guided network function," 2024.
- [4] A. Mallya and S. Lazebnik, "Packnet: Adding multiple tasks to a single network by iterative pruning," in *IEEE Conf. on Computer Vision and Pattern Recognition*, Los Alamitos, CA, USA, jun 2018, pp. 7765–7773.
- [5] Y. Yu, X. Si, C. Hu, and J. Zhang, "A review of recurrent neural networks: Lstm cells and network architectures," *Neural computation*, vol. 31, no. 7, pp. 1235–1270, 2019.
- [6] P. J. Werbos, "Neural networks for control and system identification," Tampa, FL, USA, Dec. 1989, pp. 260–265.

- [7] B. D. Anderson and J. B. Moore, *Optimal control: linear quadratic methods*. Courier Corporation, 2007.
- [8] B. Kouvaritakis and M. Cannon, "Model predictive control," *Switzerland: Springer International Publishing*, vol. 38, pp. 13–56, 2016.
- [9] J. P. Hespanha, D. Liberzon, and A. S. Morse, "Overcoming the limitations of adaptive control by means of logic-based switching," *Systems & Control Letters*, vol. 49, no. 1, pp. 49–65, 2003.
- [10] K. J. Åström, "Adaptive control," in *Mathematical System Theory: The Influence of R. E. Kalman*, A. C. Antoulas, Ed. Springer Berlin Heidelberg, 1991, pp. 437–450.
- [11] B. Mårtensson, "The order of any stabilizing regulator is sufficient a priori information for adaptive stabilization," *Systems & Control Letters*, vol. 6, no. 2, pp. 87–91, 1985.
- [12] M. Fu and B. Barmish, "Adaptive stabilization of linear systems via switching control," *IEEE Transactions on Automatic Control*, vol. 31, no. 12, pp. 1097–1103, 1986.
- [13] D. Miller and E. Davison, "An adaptive controller which provides an arbitrarily good transient and steady-state response," *IEEE Transactions on Automatic Control*, vol. 36, no. 1, pp. 68–81, 1991.
- [14] L. Xin, L. Ye, G. Chiu, and S. Sundaram, "Identifying the dynamics of a system by leveraging data from similar systems," Atlanta, GA, USA, Jun. 2022, pp. 818–824.
- [15] Y. Chen, A. M. Ospina, F. Pasqualetti, and E. Dall'Anese, "Multi-task system identification of similar linear time-invariant dynamical systems," Marina Bay Sands, Singapore, Dec. 2023, to appear. arXiv preprint arXiv:2301.01430.
- [16] T. T. Zhang, K. Kang, B. D. Lee, C. Tomlin, S. Levine, S. Tu, and N. Marni, "Multi-task imitation learning for linear dynamical systems," *arXiv preprint arXiv:2212.00186*, 2022.
- [17] T. Guo, A. A. Al Makdah, V. Krishnan, and F. Pasqualetti, "Imitation and transfer learning for LQG control," vol. 7, pp. 2149–2154, 2023.
- [18] B. Richards, D. Tsao, and A. Zador, "The application of artificial intelligence to biology and neuroscience," *Cell*, vol. 185, no. 15, pp. 2640–2643, 2022.
- [19] G. I. Parisi, R. Kemker, J. L. Part, C. Kanan, and S. Wermter, "Continual lifelong learning with neural networks: A review," *Neural Networks*, vol. 113, pp. 54–71, 2019.
- [20] M. Soare, O. Alsharif, A. Lazaric, and J. Pineau, "Multi-task linear bandits," in *NIPS2014 Workshop on Transfer and Multi-task Learning: Theory meets Practice*, 2014.
- [21] A. A. Deshmukh, U. Dogan, and C. Scott, "Multi-task learning for contextual bandits," in *Advances in Neural Information Processing Systems*, vol. 30. Curran Associates, Inc., 2017, pp. 4851–4859.
- [22] D. Kavranoglu, M. Bettayeb, and M. F. Anjum, " $\mathcal{L}_\infty$  norm simultaneous system approximation," vol. 6, no. 9–10, pp. 999–1014, 1996.
- [23] S. Guerra-Gomes, N. Sousa, L. Pinto, and J. F. Oliveira, "Functional roles of astrocyte calcium elevations: From synapses to behavior," *Frontiers in Cellular Neuroscience*, vol. 11, p. 427, 2018.
- [24] C. H. T. Tran, G. Peringod, and G. R. Gordon, "Astrocytes integrate behavioral state and vascular signals during functional hyperemia," *Neuron*, vol. 100, no. 5, pp. 1133–1148.e3, 2018.
- [25] C. Murphy-Royal, S. Ching, and T. Papouin, "A conceptual framework for astrocyte function," vol. 26, no. 11, pp. 1848–1856, 2023.
- [26] J. Vanbiervliet, B. Vandereycken, W. Michiels, S. Vandewalle, and M. Diehl, "The smoothed spectral abscissa for robust stability optimization," vol. 20, no. 1, pp. 156–171, 2009.
- [27] K. B. Petersen and M. S. Pedersen, *The Matrix Cookbook*. Technical University of Denmark, 2012.
- [28] K. J. Åström and R. M. Murray, *Feedback Systems*, 2008.
- [29] M. S. Tombs and I. Postlethwaite, "Truncated balanced realization of a stable non-minimal state-space system," *International Journal of Control*, vol. 46, pp. 1319–1330, 1987.
- [30] A. C. Antoulas and D. C. Sorensen, "Approximation of large-scale dynamical systems: an overview," *Int. J. Applied Mathematics and Computer Science*, vol. 11, no. 5, pp. 1093–1121, 2001.
- [31] R. M. Corless, G. H. Gonnet, D. E. G. Hare, D. J. Jeffrey, and D. E. Knuth, "On the lambert w function," *Advances in Computational Mathematics*, vol. 5, no. 1, pp. 329–359, 1996.